Volume 1 | Number 1 | Jan 2013 | Pages 1–100

CrystEngComm

www.rsc.org/crystengcomm

ROYAL SOCIETY OF CHEMISTRY

ROYAL SOCIETY OF CHEMISTRY

www.rsc.org/crystengcomm

Rhodium Growth on Cu$_2$S Nanocrystals Yielding Hybrid Nanoscale Inorganic Cages and Their Synergetic Properties

Kathy Vinokurov[1,3], Yehonadav Bekenstein[2,3], Vitaly Gutkin[3], Inna Popov[3], Oded Millo[2,3] and Uri Banin[1,3*]

[1] The Institute of Chemistry, The Hebrew University of Jerusalem, Jerusalem 91904, Israel

[2] Racah Institute of Physics, The Hebrew University of Jerusalem, Jerusalem 91904, Israel

[3] The Center for Nanoscience and Nanotechnology, The Hebrew University of Jerusalem, Jerusalem 91904, Israel

* E-mail: uri.banin@mail.huji.ac.il

Abstract

Metal decoration on the edges of highly faceted Cu$_2$S semiconductor nanocrystals yields a family of Nano-Inorganic Caged (NICed) semiconductor-metal hybrid nanoparticles. We present growth of Rhodium and of Ruthenium-Rhodium mixture to give Rh-Cu$_2$S and RuRh-Cu$_2$S hybrid nanoparticle cages, respectively. Transmission electron microscopy affirms the growth of the metals selectively on the nanocrystal edges, within a narrow temperature window. The oxidation level of the metal frame could be also controlled during the reaction stages as characterized by X-ray photoelectron spectroscopy, providing additional variation for the hybrid nanoparticle cages. The synergetic electronic properties of the hybrid nanocages were observed on single particle level using scanning tunneling spectroscopy. The various cage nanoparticles are also of interest as possible catalysts for metal and metal-oxide catalyzed reactions.

1

1. Introduction

The combination of two or more disparate materials on a single nanoparticle provides a powerful strategy for creating different hybrid structures with multiple properties stemming from the constituents and their interactions.[1-3] This has been exemplified by the combination of metals with a semiconductor nanocrystal providing synergetic electronic properties at the unique metal-semiconductor nanoscale interface as well as light induced charge separation effects. The combined and often synergetic properties render potential for use of hybrid semiconductor-metal nanoparticles in various applications, including photocatalysis,[4] catalysis,[5] photovoltaics[6] and nano-electronic devices.[7-9]

An intriguing hybrid nanoparticle is that of a cage architecture. The first example of a hybrid nano-inorganic cage (NIC) structure, was composed of a Cu_2S nanocrystal seed overcoated by a Ru metal frame.[10, 11] A unique Ru metal edge growth mechanism was revealed and found to be highly sensitive to the reaction temperature. The cage growth phase took place only in a narrow window of $205\pm2°C$, while at the range of 190-220°C the Ru growth evolved leading to different growth patterns. This was assigned to the temperature dependent interplay of homogeneous versus heterogeneous nucleation of Ru. It was suggested further that a change within surface ligands of the seed occurring at the cage growth temperature provides the necessary conditions of increased reactivity of the seed nanocrystal edges for the unique edge growth. At lower temperature of 190°C, homogeneous nucleation of Ru via reduction by the amine solvent was preferred over heterogeneous nucleation of Ru via reduction by Cu^{1+} on the Cu_2S seed surface. At the temperature range of 210–220°C both heterogeneous and homogeneous nucleation routes can take place, developing into

vermicular structures, either by Ru growing from the metal nuclei on the seed edge or from the coalescence of free Ru particles in the reaction medium with these nuclei. Edge growth, therefore, occurs only within the narrow temperature region around 205°C, and is related to the structure of the highly facetted seed nanocrystal, leading to the higher reactivity of the edge region emphasized in this particular temperature region.

It is of interest to further expand this type of edge growth on Cu_2S seeds also to additional metals, also opening a route for bi-metal hybrid NICs. This can also contribute to further applicability of these systems, in particular in catalysis, since the transition metals including ruthenium and rhodium nanoparticles, and their oxidized forms, have been extensively demonstrated as effective catalysts in different applications. Their catalytic activity is dependent on size, oxidation state and shape. For example, Rh_2O_3 shows semimetallic or semiconducting behavior.[12] As such it is a good candidate for different catalytic reactions.[13] One of the main studies on Rh_2O_3 catalytic properties is in the decomposition reaction of Nitrous oxide, which is of environmental importance. The rhodium oxide catalyst showed enhanced activity assigned to decreasing the activation energy of the N-O bond splitting.[14] Another promising use of Rh_2O_3 catalyst is in the field of CO oxidation.[15] Its catalytic activity was shown to give similar behavior to Pt nanoparticles supported on γ-Al_2O_3.[16] Furthermore, Rh_2O_3 nanoparticles, anchored to the surface of Nb oxide layer, were reported as very effective catalysts in the photocatalytic reaction of hydrogen generation using methanol as a hydrogen donor. [17]

Catalysts composed of two metals, can promote the catalytic reaction to an advanced level through various effects including the decrease of the amount of the more expensive metal component, overcoming the catalysts poisoning with one of the

products, and also by promoting parallel reactions. For example, in the methanol oxidation reaction, the combination of Pt and Ru metals was found to meet these requirements.[18]

Here we report on selective edge growth of Rh and the mixture of Ru-Rh onto Cu_2S nanocrystal seeds to extend the selection of hybrid cage nanoparticles that are of relevance for different catalytic applications. We address the optimal reaction conditions to achieve the growth of mono- and bi-metal NICs. Structural characterization was performed and also Rh metal frame was further examined by emptying the semiconducting interior of the cage. The composition of bi-metal frame was studied by Energy Dispersive X-ray Spectroscopy (EDX) – elemental mapping analysis, showing homogeneous distribution both of Ru and Rh on the Cu_2S seed edges. Additionally, the metal oxidation state was addresses by X-ray Photoelectron Spectroscopy (XPS) technique. The XPS analysis sheds light on derivatives of the cage frames, and its tendency to be oxidized by various environmental conditions. The electronic properties were studied by Scanning Tunneling Microscopy (STM) revealing synergistic behavior of the metal-semiconductor junctions within the hybrid cages.

2. Experimental

2.1. Materials synthesis

Rh growth on the edges of highly faceted copper(I) sulfide nanoparticles is performed based on the procedure reported previously with minor modifications (Figure 1 a-b).[10, 11] The 14nm hexagonal truncated biprism Cu_2S seeds are synthesized according to literature[19] and are thoroughly cleaned in chloroform from the excess amount of ligands. Afterwards, the nanocrystal seeds are re-dispersed in 2g octadecylamine and then heated to 205°C. At the same time, the stock precursor

4

solution of Rhodium acetylacetonate (Rh(acac)$_3$) in diphenylether and dichlorobenzene (volume ratio 3.2 to 1, respectively) is also heated to the same temperature. Then a quick injection of the precursor solution to the seed solution is performed. The selective edge growth is achieved by keeping the reaction temperature fluctuations within ±2°C, both during the injection and during the growth process which proceeds for half an hour. The reaction product, hybrid nanocages, is precipitated by addition of hot isopropanol and separated by centrifugation at 5000 rpm for 5min. The precipitate was washed and centrifuged three additional times and redispersed in chloroform. All the mentioned workup processes were carried out in air or in the glove box and the specific conditions can influence the oxidation rate of the metal frame. Moreover, rhodium growth was further expanded to a bi-metal system. In this case, Ru and Rh stock solution was prepared by mixing equimolar amounts of Ru(acac)$_3$ and Rh(acac)$_3$ in diphenylether and dichlorobenzene solvents (volume ratio 3.2 to 1, respectively). The precursor solution was heated to 205°C and swiftly injected into the Cu$_2$S seeds solution, which was kept at the same temperature. The reaction was carried out under Ar and stirred for 30min.

2.2 Materials Characterization

Structural characterization of the hybrid nanoparticles was carried out by Tecnai F20 G2 High-Resolution TEM (HRTEM) using both HRTEM and High Angle Annular Dark Field-Scanning TEM (HAADF-STEM). Samples for TEM were prepared by deposition of a drop of particle chloroform solution onto a carbon-coated copper/nickel grid. The composition of RuRh-Cu$_2$S hybrid nanocage was characterized using Energy Dispersive X-ray Spectroscopy (EDX) – elemental mapping analysis. X-ray Photoelectron Spectroscopy (XPS) measurements were recorded on Kratos AXIS Ultra X-ray photoelectron spectrometer (Kratos Analytical,

Manchester, UK). Spectra were acquired using the Al-Kα monochromatic X-ray source (1,486.7 eV) with 0° take of angle (normal to the analyzer). The electronic properties of hybrid cages were measured by Scanning Tunneling Microscopy (STM) at room temperature under high vacuum, using Pt-Ir tips. For more details on XPS and STS techniques see the Supplementary Information (SI).

3. **Results and Discussion**

We first address modifications of the Rh growth conditions with respect to our earlier work on Ru growth on the Cu_2S seed nanocrystals. The $Ru(acac)_3$ precursor used in our previous reports on Ru-Cu_2S NICs, dissolved well in dioctylether and was stable in this solvent for elongated time. However, in this solvent, with $Rh(acac)_3$ precursor, a dark precipitate was observed during heating, which we attribute to reduction of the metal. Hence, a first aspect that was addressed upon changing to Rh, relates to the precursor solution solvent, to offer a stable solution up to the reaction temperature (~205°C). A selection of solvents was examined in this context, starting with ethers. Diphentylether was chosen since at room temperature both $Rh(acac)_3$ and $Ru(acac)_3$ dissolved well and remain stable also at high temperature. However, this solvent is volatile at high temperatures and therefore difficult to use. To address this, a mixture of diphenlyether and dichlorobenzene (volume ratio 3.2 to 1, respectively) was chosen as an optimal solvent.

Selective growth of Rh and Ru-Rh metals on the crystal edges of 14 nm Cu_2S seeds was characterized by High-Resolution TEM (HRTEM) and High Angle Annular Dark Field-Scanning TEM (HAADF-STEM) (Figure 1). Patterns of darker and lighter contrast regions were observed in the TEM images (Figure 1a,c). The lighter regions are related to the Cu_2S semiconductor interior, while darker ones are attributed to Rh and Ru, the materials with higher atomic number. Due to the

truncated hexagonal biprism structure of the seed,[20] it might have various orientations on the TEM grid further influencing the location of darker areas attributed to the metal. The HAADF-STEM measurements (Figure 1b,d) support the TEM observations regarding the formation of cage like structures. In this Z-contrast imaging technique, the metal gives much stronger signal leading to brighter patterns on the hybrid nanoparticles.

A study of the selective metal growth processes on the edges of 14 nm faceted copper(I) sulfide seeds revealed dependence on several conditions. This includes the seed degree of separation from the organic matrix, the molar ratio of metal precursor to copper in the Cu_2S seed, and the reaction temperature. Insufficient cleaning of the seed from excess organic ligands, can lead to inconsistencies in the amount of metal precursor to be consumed in the cage growth step. An optimal growth temperature of the cage at 205°C was found also in this case, while temperature fluctuation within ±5°C can lead to additional growth modes of the metals as we have described in our previous work.[11]
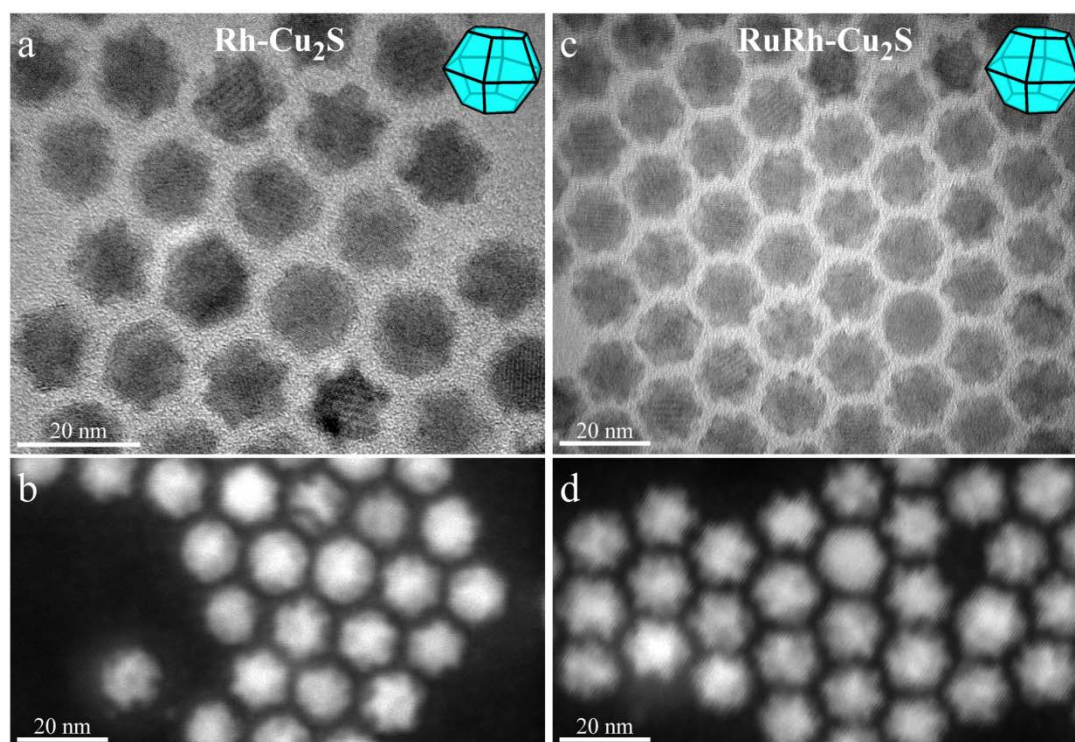
Figure 1: TEM characterization of Rh-Cu$_2$S nano-inorganic cages (a-b), and RuRh-Cu$_2$S nano-inorganic cages (c-d). a,c - HRTEM images of Rh-Cu$_2$S hybrid cages, and RuRh-Cu$_2$S bi-metal hybrid cages respectively. Darker regions are assigned to the metal frame due to the higher electron density in those regions. b,d – HAADF-STEM images of the corresponding cage structured nanocrystals. Lighter regions are with higher scatter in consistency with the Z-contrast imaging principle where the higher Z metals are providing stronger signal.

There is also a possibility to selectively empty the Cu$_2$S interior, by leaching out copper(I) ions with neocuproine/phenanthroline Cu chelating ligand,[19] while leaving behind the metal frame of the cage intact. This is an interesting structure for catalysis, due to the presence of high surface area and voids (Figure 2). The rhodium cage framework was studied by TEM (Figure 2a) and its hollow structure was clearly observed also by HAADF-STEM (Figure 2d). Rh crystalline phase was characterized by selected area electron diffraction (SAED), showing orthorhombic crystalline structure of rhodium oxide (Figure 2f). The observed fully oxidized cage frame with

the oxidized form of Rh_2O_3 might occur due to several effects. First, during the metal growth stage, oxidizing derivatives of the metal precursor may form, in analogy to previous report on various metal-(acac)$_3$ species previously.[21] Second, during the cage workup procedure followed by the emptying of the seed interior. Both workup and cage emptying processes were carried out under ambient conditions.
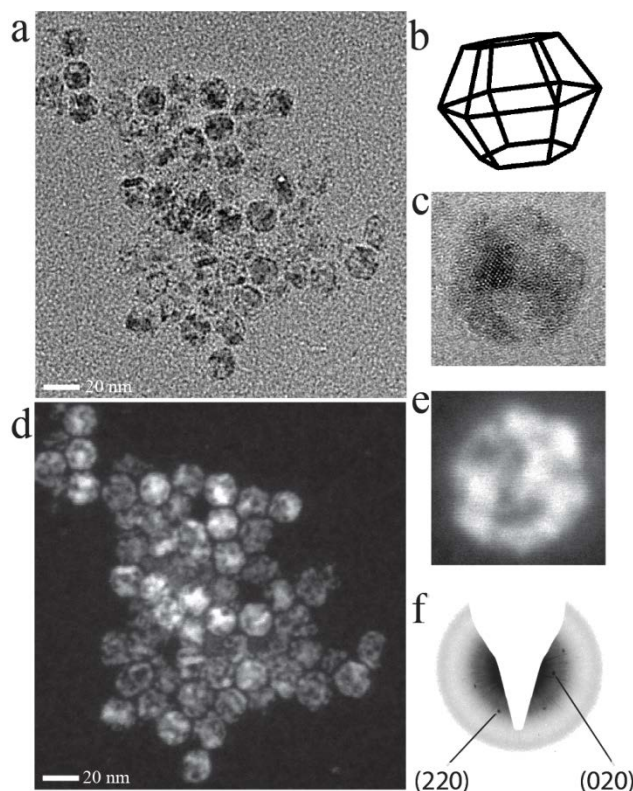
Figure 2: Rh empty cages obtained from the hybrid nanoparticles. a - HRTEM images of Rh containing cage. b – cartoon of the truncated hexagonal biprism shape. c – close up of HRTEM image of Rh metal cage. d – HAADF-STEM images of the corresponding cage structured Rh crystals. e - close up of HAADF-STEM images of Rh metal cage. f - SAED with broad reflections indexed to orthorhombic Rh_2O_3 of empty Rh NICs.

Characterizing the metal frame composition is important both for understanding the reaction mechanism and is also a determining factor for the catalytic properties.

To further characterize the Rhodium nanomteric frame and its tendency for oxidation, X-ray Photoelectron Spectroscopy (XPS) was used (for technical details see Supplementary Information (SI)). For the XPS study, monolayers of hybrid nanoparticles were bound to a gold surface using 1,6-hexanedithiol as a linker compound.[22-24] The XPS study was done on Rh hybrid cages, comparing workup conditions in air versus inert atmosphere. These observations were further clarified by additionally analyzing by XPS Ru and RuRh hybrid cages.

For Rh cages, which were washed up under air and exposed to technical grade isopropanol, we have observed that the product frame was fully oxidized to give almost exclusively a peak which matches the oxidation level for Rh_2O_3 (Figure S1 in the SI). This was compared with Ru-Cu_2S NICs, which have well established synthesis procedure and were characterized in our previous work. The Ru cage sample was also exposed to air during the workup procedure.[11] The XPS measurements showed combination of components with oxidation states corresponding to Ru(0) and RuO_2 constructing the metallic frame (Figure S3 in the SI). Ru(0) was found to be the dominant component, consistent with previous XRD results showing Ru(0) metal frame. The relatively low amounts of RuO_2 traces in XPS are assigned to surface layer oxidation during the workup procedure under air.

The Rh cages were also examined in the case where the crude product treatment was carried out in the glove box using anhydrous isopropanol. Even in this case a large component of rhodium oxide was still observed, but now also accompanied by a smaller component of Rhodium(0) (Figure S2 in the SI). This significant partial oxidation even in inert workup conditions, is assigned to the sensitivity of Rh to oxidation by oxidizing agents formed due to degradation of the (acac) during the synthesis of the metal frame. Previous study on thermal decomposition of metal

acetylacetonates has shown that acidic compounds can be formed from chelating ligands[21] surrounding the central atom in an octahedral arrangement.[25] Moreover, it was already shown that Rh nanoparticles will oxidize both under air and Ar environment, whereas crystals synthesized under air will contain a larger amount of oxidized derivatives,[26] consistent with observations in our system.

The next step was to examine the oxidation tendency of each metal component in RuRh-Cu$_2$S bi-metal hybrid cages exposed to air during the product workup. In the survey spectrum (Figure 3a), Ru and Rh are observed along with peaks assigned to Cu and S from the seed particles. The higher tendency towards oxidation of rhodium versus ruthenium is observed. In the case of Rh, a large component of Rh$_2$O$_3$ is seen, with small contribution from Rh(0) (Figure 3b). Ru, on the other hand, showed dominant component of Ru(0) with a small component of RuO$_2$ (Figure 3c). The ratios among the compounds are summarized in Table S1 (see the Supplementary Information).
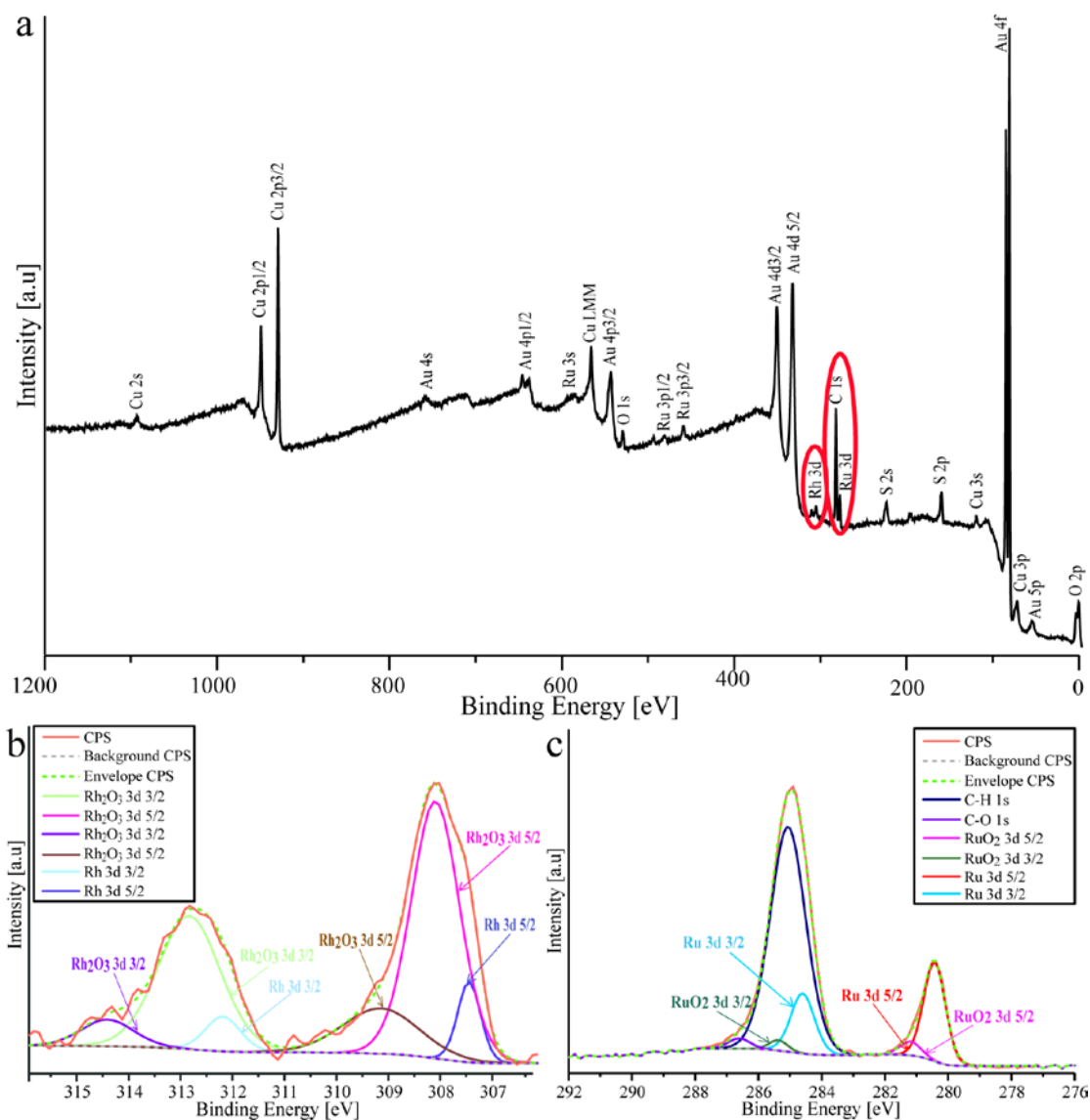
Figure 3: XPS data of RuRh-Cu$_2$S bi-metal hybrid cages. a – XPS survey spectra of RuRh-Cu$_2$S hybrid cage layer bound to gold through 1,6-hexanedithiol. The marked area is related to the peaks of Ru and Rh. b – High resolution XPS spectra for Rh 3d$_{5/2}$ and Rh 3d$_{3/2}$ peaks, with fits for Rh(0) and Rh$_2$O$_3$ components decorating Cu$_2$S edges. c – High resolution XPS spectra for Ru 3d$_{5/2}$ and Ru 3d$_{3/2}$ peaks (overlapping with C 1s peaks). Dominant Ru(0) component is observed, with minor contribution of RuO$_2$.

The composition of bi-metal hybrid nanocages was further characterized and mapped by Energy Dispersive X-ray Spectroscopy (EDX) – elemental mapping analysis using STEM (Figure 4). The marked area with a red square (Figure 4a) was

12

scanned, detected by CCD camera, while elemental characterization was carried out as well. The EDX chemical characterization yielded four components - Cu, S, Ru and Rh - comprising the analyzed cage area (Figure 4c-f). Copper and sulfur exhibit a homogeneous distribution, as is expected for the 14nm Cu_2S seed (Figure 4c,d), whereas ruthenium and rhodium enrichment is found on the edges, consistent with selective edge growth of the metals (Figure 4e,f).[10, 11]
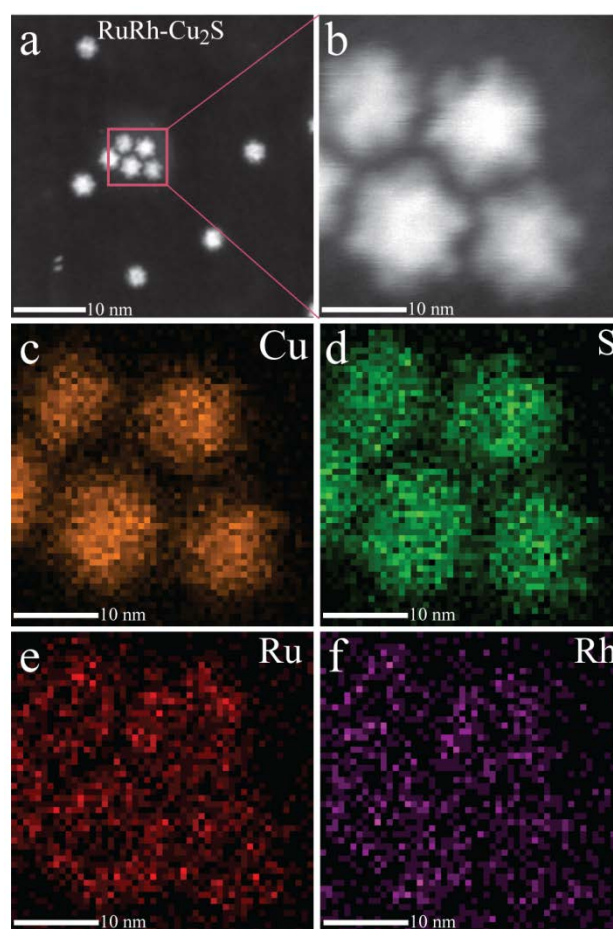
Figure 4: EDX elemental mapping analysis of RuRh-Cu_2S nano-inorganic cages. A) HAADF-STEM image of bi-metal hybrids. B)_ zoom-in on the particles area that was scanned and analyzed. c-f – mapping results for Cu (frame c), S (frame d), Ru (frame e), and Rh (frame f) RuRh-Cu_2S bi-metal nanocages, suggesting that the semiconductor components are homogeneously distributed (Cu and S) while the metals are on the edges.

To study the combined and possibly synergetic electronic properties of the cages, they were studied by Scanning Tunneling Microscopy (STM) and Spectroscopy (STS). Dilute samples of the cages were deposited on atomically flat Au surfaces, where isolated NC can be measured. The STM tip was positioned above a single cage realizing a double barrier tunnel junction configuration, and I-V spectra were acquired. Specific sample preparation details and additional measurement parameters can be found in the SI.

Figure 5a presents the dI/dV-V spectra measured on RuRh-Cu_2S NICs. The different curve colors represent various tip positions on the nanoparticle. The red curve shows typical semiconductor behavior on the seed facets with a band gap of ~1.4eV, which is in good agreement to the bare Cu_2S energy gap value.[27] The black curve shows the behavior of the cage metallic edge, as is expected for metal nanoparticles with a Coulomb blockade and staircase features. The blue curve is assigned to the metal-semiconductor interface with finite conductance at zero bias indicating the existence of in-gap states which are a hallmark of the synergistic properties of the hybrid structure.[28]

Valuable insight can be attained from the statistical histograms of the data sets. A full compilation of the zero energy gap values extracted from the STS results is presented in two panels for the aforementioned four different NC types. The results for the measured Ru-Cu_2S and Rh-Cu_2S NICs, metal Ru cages and bare Cu_2S seeds, are presented in Figure 5b,c. The first histogram (Figure 5b) presents the relative abundance of zero bias gap values of metallic ruthenium cages (blue bars) and of Cu_2S semiconducting seeds (red bars). For the Cu_2S semiconducting seeds, band gap values of ~1.4eV are observed, similar to previous reported values for the band gap of the material and in particular for such seeds from our previous study. The small gap

values observed for the empty Ru cages (<0.3eV) are interpreted as Coulomb blockade gaps for these structures. The second histogram (Figure 5c) presents gap values measured on the hybrid population both for the Ru (green bars) and Rh (brown bars) NICs, which show a distribution of values covering the range from the low values corresponding to Coulomb blockade gaps, to the larger values corresponding to the Cu_2S band gap. In addition, in the hybrid NICs, intermediate values in the range of 0.5-1eV are detected. These are assigned to in-gap states related either to surface states formed during metal growth, or to metal-induced gap state in the semiconductor regions of the NICs.
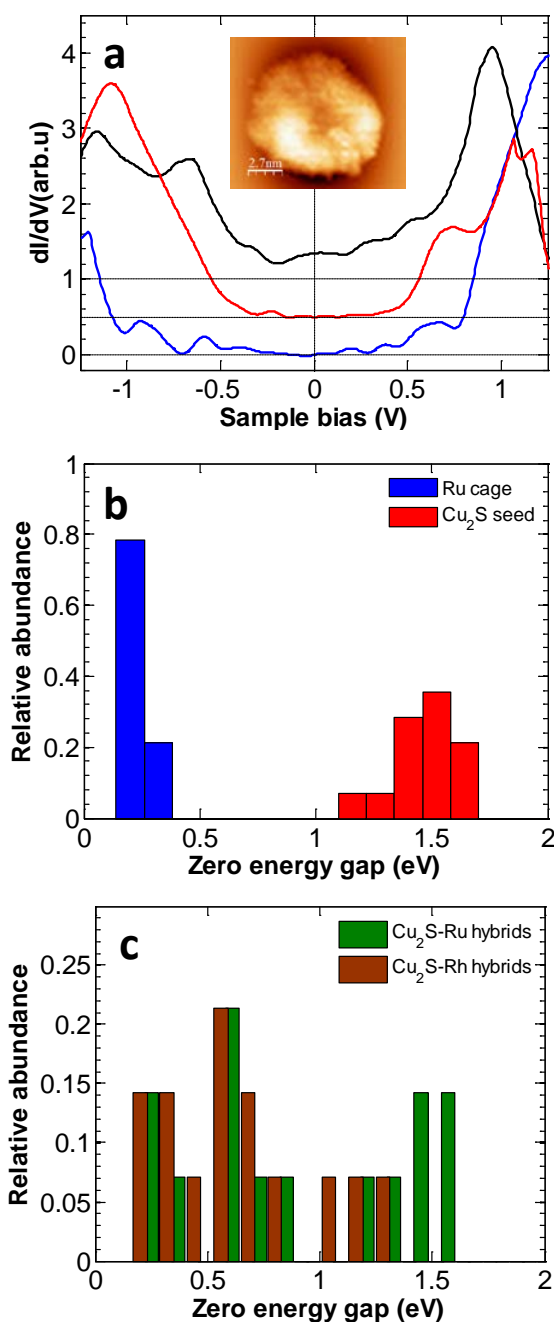
Figure 5: a - Tunneling spectra dI/dV-V measured at room temperature on the RuRh-Cu$_2$S hybrid cage, (a inset) scanning tunneling (STM) topography micrograph of the hybrid structure depicting higher conductance at the edges of the nanoparticle where metallic like RuRh-Cu$_2$S was grown. Scale bar for the STM image is 5 nm. Color scale range is 0–10 nm. Spectra obtained along different positions on the hybrid structure displayed qualitative different behavior. In some tip positions single electron

tunneling effects typical for metallic nanoparticles, namely the Coulomb blockade and staircase were observed (blue and black curves). Where on other tip positions larger band-gaps which correlate with reported Cu_2S semiconducting gap value were measured (red curve). In some cases finite conductance at zero bias (blue curve) indicated the existence of in-gap states which are a hallmark of the synergistic properties of the hybrid structure. Histograms showing the relative abundance of zero bias gap values measured on b - the bare Cu_2S seeds (red bars) and the empty Ru cages (blue bars).The small gap values (<0.3eV) are interpreted as Coulomb blockade gaps. c - Gap values measured on the hybrid population both for the Ru and Rh hybrids show intermediate values (0.5-1eV) and originate due to in-gap states.

Summary and Conclusions

Our study on growth of different metals on Cu_2S nanocrystal seeds, yielded both mono and bi-metal hybrid nano inorganic cages, including $Rh-Cu_2S$ and $RuRh-Cu_2S$ NICs. The bi-metal cage was found to be composed of components with oxidation state 0, as well as oxidized components. Different sensitivity of ruthenium and rhodium components to oxidation was observed. This observation may be of relevance in catalytic studies with such cage structures, since both rhodium metal and oxidized rhodium form have different catalytic properties, promoting the possibility to utilize their functionality. The synergetic electronic properties of the cages were studied also by scanning tunneling spectroscopy.

Acknowledgments

Supplementary Information

† Electronic Supplementary Information (ESI) available: [comment on XPS data fittings; XPS analysis of Rh-Cu$_2$S and Ru-Cu$_2$S hybrid cages; summary table of XPS data regarding RuRh-Cu$_2$S hybrid cages.] See DOI: 10.1039/b000000x/

References

1. U. Banin, Y. Ben-Shahar and K. Vinokurov, *Chemistry of Materials*, 2014, **26**, 97-110.
2. R. Costi, A. E. Saunders and U. Banin, *Angewandte Chemie-International Edition*, 2010, **49**, 4878-4897.
3. L. Carbone and P. D. Cozzoli, *Nano Today*, 2010, **5**, 449-493.
4. M. B. Wilker, K. J. Schnitzenbaumer and G. Dukovic, *Isr J Chem*, 2012, **52**, 1002-1015.
5. S. M. Kim, S. J. Lee, S. H. Kim, S. Kwon, K. J. Yee, H. Song, G. A. Somorjai and J. Y. Park, *Nano Letters*, 2013, **13**, 1352-1358.
6. M. Gratzel, *Nature*, 2001, **414**, 338-344.
7. A. Figuerola, I. R. Franchini, A. Fiore, R. Mastria, A. Falqui, G. Bertoni, S. Bals, G. Van Tendeloo, S. Kudera, R. Cingolani and L. Manna, *Advanced Materials*, 2009, **21**, 550-+.
8. P. Li, A. Lappas, R. Lavieville, Y. Zhang and R. Krahne, *Journal of Nanoparticle Research*, 2012, **14**.
9. R. Lavieville, Y. Zhang, A. Casu, A. Genovese, L. Manna, E. Di Fabrizio and R. Krahne, *Acs Nano*, 2012, **6**, 2940-2947.
10. J. E. Macdonald, M. Bar Sadan, L. Houben, I. Popov and U. Banin, *Nature Materials*, 2010, **9**, 810-815.
11. K. Vinokurov, J. E. Macdonald and U. Banin, *Chemistry of Materials*, 2012, **24**, 1822-1827.
12. J. Hamalainen, F. Munnik, M. Ritala and M. Leskela, *Journal of the Electrochemical Society*, 2009, **156**, D418-D423.
13. A. Bueno-Lopez, I. Such-Basanez and C. Salinas-Martinez de Lecea, *Journal of Catalysis*, 2006, **244**, 102-112.
14. F. Kapteijn, J. RodriguezMirasol and J. A. Moulijn, *Applied Catalysis B-Environmental*, 1996, **9**, 25-64.
15. F. S. Lai and B. C. Gates, *Nano Letters*, 2001, **1**, 583-587.
16. M. J. Kahlich, H. A. Gasteiger and R. J. Behm, *Journal of Catalysis*, 1997, **171**, 93-105.
17. H. Hata, Y. Kobayashi, V. Bojan, W. J. Youngblood and T. E. Mallouk, *Nano Letters*, 2008, **8**, 794-799.

18. G. R. Salazar-Banda, K. I. B. Eguiluz, M. M. S. Pupo, H. B. Suffredini, M. L. Calegaro and L. A. Avaca, *Journal of Electroanalytical Chemistry*, 2012, **668**, 13-25.
19. W. Han, L. Yi, N. Zhao, A. Tang, M. Gao and Z. Tang, *Journal of the American Chemical Society*, 2008, **130**, 13152-13161.
20. F. Zhao, X. Chen, N. Xu, P. Lu, J.-G. Zheng, Q. Su and M. Wu, *Journal of Physics and Chemistry of Solids*, 2006, **67**, 1786-1791.
21. J. V. Hoene, R. G. Charles and W. M. Hickam, *The Journal of Physical Chemistry*, 1958, **62**, 1098-1101.
22. V. L. Colvin, A. N. Goldstein and A. P. Alivisatos, *Journal of the American Chemical Society*, 1992, **114**, 5221-5230.
23. C. Palegrosdemange, E. S. Simon, K. L. Prime and G. M. Whitesides, *Journal of the American Chemical Society*, 1991, **113**, 12-20.
24. C. D. Bain, J. Evall and G. M. Whitesides, *Journal of the American Chemical Society*, 1989, **111**, 7155-7164.
25. G. K. J. Chao, R. L. Sime and R. J. Sime, *Acta Crystallographica Section B*, 1973, **29**, 2845-2849.
26. Y. Zhang, M. E. Grass, S. E. Habas, F. Tao, T. Zhang, P. Yang and G. A. Somorjai, *Journal of Physical Chemistry C*, 2007, **111**, 12243-12253.
27. J. M. Luther, P. K. Jain, T. Ewers and A. P. Alivisatos, *Nature Materials*, 2011, **10**, 361-366.
28. Y. Bekenstein, K. Vinokurov, U. Banin and O. Millo, *Nanotechnology*, 2012, **23**, 505710.

TOC

Edge growth of rhodium and ruthenium-rhodium metals on highly faceted semiconductor Cu_2S seeds yields a family of nano-inorganic caged hybrid nanoparticles.